

The following publication Al-Busaidi, I. J., Haque, A., Al-Balushi, R. A., Rather, J. A., Munam, A., Ilmi, R., ... & Khan, M. S. (2021). Synthesis, characterization, and optoelectronic properties of phenothiazine-based organic co-poly-ynes. *New Journal of Chemistry*, 45(33), 15082-15095 is available at <https://doi.org/10.1039/d1nj00925g>.

## **Synthesis, characterization, and optoelectronic properties of phenothiazine-based organic co-poly-ynes**

Idris Juma Al-Busaidi,<sup>1</sup> Ashanul Haque,<sup>2\*</sup> Rayya Al-Balushi,<sup>3</sup> Jahangir Ahmad Rather,<sup>1</sup> Abdul Munam,<sup>1</sup> Rashid Ilmi,<sup>1</sup> Paul R. Raithby,<sup>4\*</sup> Youming Zhang,<sup>5</sup> Yingying Fu,<sup>7</sup> Zhiyuan Xie,<sup>7\*</sup> Shuming Chen,<sup>8\*</sup> Shahidul M Islam,<sup>9</sup> Wai-Yeung Wong,<sup>5\*</sup> Jonathan M. Skelton,<sup>6\*</sup> Muhammad S. Khan<sup>1\*</sup>

<sup>1</sup> Department of Chemistry, Sultan Qaboos University, P.O. Box 36, Al-Khod 123, Sultanate of Oman.

<sup>2</sup> Department of Chemistry, College of Science, University of Hail, Ha'il 81451, Kingdom of Saudi Arabia.

<sup>3</sup> Department of Basic Sciences, College of Applied Sciences and Health Sciences, A'Sharqiyah University, Ibra 400, Sultanate of Oman.

<sup>4</sup> Department of Chemistry, University of Bath, Bath BA2 7AY, U.K.

<sup>5</sup> Department of Applied Biology and Chemical Technology and Research Institute for Smart Energy, The Hong Kong Polytechnic University, Hung Hom, Kowloon, Hong Kong, P. R. China.

<sup>6</sup> Department of Chemistry, University of Manchester, Oxford Road, Manchester M13 9PL, U.K.

<sup>7</sup> State Key Laboratory of Polymer Physics and Chemistry, Changchun Institute of Applied Chemistry, Chinese Academy of Sciences, Changchun 130022, P. R. China.

<sup>8</sup> Department of Electrical and Electronic Engineering, Southern University of Science and Technology, Shenzhen, 518055, P. R. China.

<sup>9</sup> Department of Chemistry, University of Illinois at Chicago, Chicago, IL 60607.

\* Corresponding authors. E-mail: Ashanul Haque: [a.haque@uoh.edu.sa](mailto:a.haque@uoh.edu.sa) (AH)  
Paul R. Raithby: [p.r.raithby@bath.ac.uk](mailto:p.r.raithby@bath.ac.uk) (PRR)  
Zhiyuan Xie: [xiezy\\_n@ciac.ac.cn](mailto:xiezy_n@ciac.ac.cn) (ZYX)  
Shuming Chen: [chen.sm@sustc.edu.cn](mailto:chen.sm@sustc.edu.cn) (SMC)  
Wai-Yeung Wong: [wai-yeung.wong@polyu.edu.hk](mailto:wai-yeung.wong@polyu.edu.hk) (WYW)  
Jonathan M. Skelton: [jonathan.skelton@manchester.ac.uk](mailto:jonathan.skelton@manchester.ac.uk) (J.M.S)  
Muhammad S. Khan: [msk@squ.edu.om](mailto:msk@squ.edu.om) (MSK).

## **Abstract**

We present the synthesis and characterization of seven new organic co-poly-ynes **P1-P7** incorporating the phenothiazine (PTZ) motif and evaluate their optoelectronic properties and performance in polymer light-emitting diodes and polymer solar cells (PLEDs/PSCs). The co-poly-ynes were obtained in moderate to high yields *via* Sonogashira coupling reactions and characterized using analytical, spectroscopic and electrochemical techniques and complementary quantum-chemical modelling. The materials show strong optical absorption in the visible region of the spectrum and most also show strong emission with quantum yields in the range of 13-41 % relative to Rhodamine 6G (R6G). PLED devices based on the co-poly-ynes were prepared and the most promising was measured to have a brightness of up to  $1.10 \times 10^4$  cd m<sup>-2</sup>. PSCs based on donor materials incorporating some of the polymers were prepared and demonstrated power conversion efficiencies of up to 0.24 %.

**Keywords:** Phenothiazine (PTZ); co-poly-ynes; optoelectronic properties, electrochemical properties; polymer light emitting diodes (PLEDs); polymer solar cells (PSCs)

## 1. Introduction

Conjugated polymers are an important class of semiconducting materials that have found application in various types of optoelectronic (OE) devices.<sup>1, 2</sup> These materials show tunable structure-dependent properties, are low cost, flexible, lightweight, and highly transparent, and are amenable to solution processing and roll-to-roll production, all of which lend themselves well to miniaturized OE devices.<sup>3</sup> Among the wide variety of polymeric systems available,  $\pi$ -conjugated poly-ynes, i.e. systems containing alternating and repeating  $-C\equiv C-$  units, have drawn considerable attention in the last few decades.<sup>4, 5</sup> Various homo-poly-ynes, hetero-copoly-ynes and metalla-polyynes incorporating carbocyclic or heterocyclic  $\pi$ -conjugated spacer groups have been reported in the literature.<sup>2, 6-8</sup> It is now unambiguously recognized that the photo-physical properties and structural features, and therefore the potential applications of these materials are largely governed by the organic spacers.<sup>7, 8</sup> For example, the introduction of electron donor (D) and acceptor (A) spacers into the main chain has been shown to be an excellent strategy for obtaining materials with extended absorption, optically-bright charge-transfer transitions, small frontier energy level differences (i.e. narrow band gaps  $E_g$ ), and good electrical conductivity.<sup>9-11</sup>

We previously found that dioctyloxyphenylene-2,3-diphenylthieno[3,4-b]pyrazine-based co-polyynes possess small band gaps ( $E_g = 1.72$  eV) and can be used as donor materials for photo-voltaic applications.<sup>12</sup> Cho and workers<sup>13</sup> demonstrated that the presence of acetylene linkages in the D-A co-polymers not only facilitates favorable orbital overlap but also enables facile transport of excitons (electron-hole pairs). Cheng and coworkers<sup>14</sup> subsequently demonstrated that the insertion of alkynyl units as side chains in a co-poly-yne greatly improved their field-effect mobility behavior. Motivated by these primary observations, researchers around the globe have since reported numerous co-polyynes and demonstrated their applications in OE devices, molecular wires, transistors, and sensors, among others.

Among various reported heterocyclic spacers, phenothiazine (PTZ) has emerged as one of the most promising donor cores.<sup>15-19</sup> The tricyclic chromophore adopts a butterfly-shaped core structure and is well known for its low cost and electroactive and photoactive nature.<sup>20, 21</sup> It has also been demonstrated that the presence of two heteroatoms make this core highly suitable for the construction of D-A materials with enhanced intramolecular charge transfer (ICT) characteristics.<sup>22</sup> Furthermore, it has recently been reported that the photostability and emission can be controlled by N substitution.<sup>23, 24</sup> We<sup>18</sup> and others<sup>25</sup> previously demonstrated that when PTZ is combined with a suitable acceptor fragment, the resulting materials are highly suitable for dye-sensitized solar cells (DSSCs) and bulk-heterojunction photovoltaic (BHJ-PV) devices.

However, while several studies have investigated PTZ-based dyads and triads,<sup>22</sup> there are presently no reports of co-poly-ynes incorporating PTZ. Motivated by this, we report herein the design and synthesis of seven new PTZ-based organic co-poly-ynes (P1-P7). We engineer narrow bandgaps by judiciously incorporating fused and non-fused heterocyclic spacer units including thiophene, 2,2'-bithiophene and thieno[3,2-b]thiophene alongside PTZ within the polymer backbone. We report a comprehensive characterization of the optoelectronic and electrochemical properties of the seven co-poly-

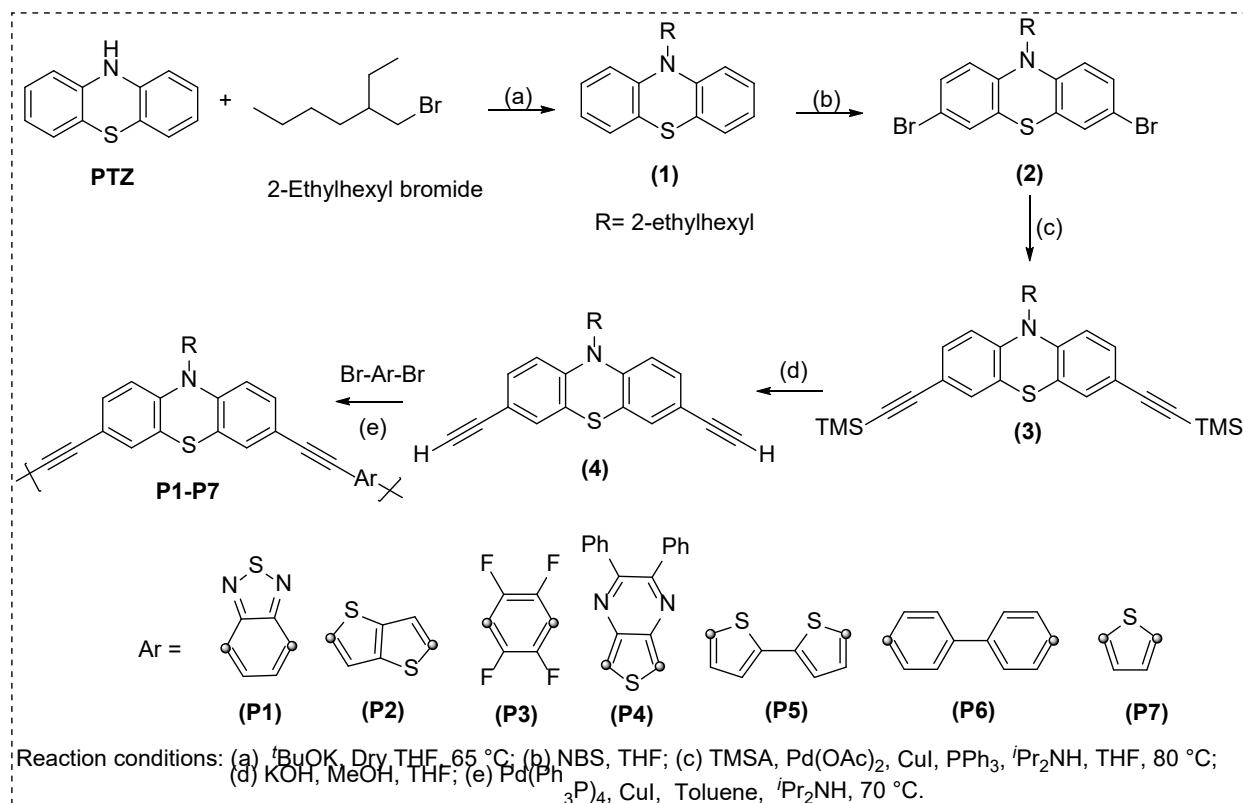
ynes, including quantum-chemical modelling using density-functional theory, and assess their performance in polymer light-emitting diode (PLED) and polymer solar cell (PSC) devices.

## 2. Results and discussion

### 2.1. Synthesis and spectroscopic characterization

The PTZ-based alkynyl ligand 10-(2-ethylhexyl)-3,7-diethynyl-10*H*-phenothiazine (**1**) was prepared in quantitative yield by reacting PTZ with 2-ethylhexyl bromide and <sup>t</sup>BuOK in THF according to previously reported procedures<sup>26</sup> (**Scheme 1**). The alkylated PTZ (**1**) was then brominated with *N*-bromosuccinimide (NBS) to obtain 3,7-dibromo-10-(2-ethylhexyl)-10*H*-phenothiazine (**2**) according to an adapted literature method.<sup>27</sup> The protected ligand precursor 3,7-bis(trimethylsilylethynyl)-*N*-(2-ethylhexyl) 10*H*-phenothiazine (**3**) was obtained by the Pd(II)/Cu(I)-catalyzed cross-coupling of the dibromo-PTZ species (**2**) and trimethylsilylacetylene (TMSA) in <sup>i</sup>Pr<sub>2</sub>NH/THF. The resulting product was deprotected using aqueous KOH in MeOH/THF and purified using silica gel column chromatography, giving 10-(2-ethylhexyl)-3,7-diethynyl-10*H*-phenothiazine (**4**) as a light-yellow viscous liquid in 95% yield. Organic co-polyynes **P1-P7** were synthesized by Sonogashira cross-coupling reactions between (**4**) and a range of dibromo aromatic spacers (Br-Ar-Br) using Pd(PPh<sub>3</sub>)<sub>4</sub>/CuI in <sup>i</sup>Pr<sub>2</sub>NH and toluene. The organic co-poly-ynes **P1-P7** were obtained in good to moderate yields (28-83 %), which were subsequently purified by alumina column chromatography followed by precipitation in CH<sub>2</sub>Cl<sub>2</sub>/methanol.

The seven co-poly-ynes were characterized by IR and <sup>1</sup>H and <sup>13</sup>C NMR spectroscopies. The IR spectra confirmed the presence of the C≡C bonds from the characteristic peaks around 2079-2210 cm<sup>-1</sup>. The <sup>1</sup>H and <sup>13</sup>C NMR spectra of the compounds showed the expected peaks corresponding to the alkyl, aryl and alkynyl fragments. Polystyrene-equivalent molecular weights (*M<sub>n</sub>*, *M<sub>w</sub>*) and polydispersity indices (PDI = *M<sub>w</sub>*/*M<sub>n</sub>*) were determined by gel permeation chromatography (GPC) using a linear polystyrene standard calibration curve. GPC provides absolute molecular weights for all of the co-poly-ynes part from **P3** and **P4**, for which the comparatively low molecular weights and the sensitivity of the multi-angle laser light scattering detector meant we could only obtain apparent molecular weights. These measurements give weight-average molecular weights in the range of (4,000-50,000 g mol<sup>-1</sup>), corresponding to weight-average degrees of polymerization (*X<sub>w</sub>*) between 13 and 213 (**Table 1**). The synthesized co-poly-ynes were found to have relatively narrow molecular weight distributions with PDIs between 1.12-1.78. These molecular weights should however be viewed with caution in view of the difficulties of using GPC to characterize rigid-rod polymers.



**Scheme 1** Preparation of the organic co-poly-yne **P1-P7**.

**Table 1** Weight- and number-average molecular weights  $M_w/M_n$ , polydispersity indices (PDIs) and degrees of polymerization  $X_w/X_n$  for the synthesized co-poly-yne **P1-P7**.

	$M_w$ ( $\text{g mol}^{-1}$ )	$M_n$	PDI	$X_w$	$X_n$
<b>P1</b>	50,100	44,600	1.12	213	190
<b>P2</b>	6,000	4,500	1.35	26	19
<b>P3</b>	4,200	2,400	1.78	18	10
<b>P4</b>	3,950	2,300	1.73	13	7
<b>P5</b>	16,900	13,800	1.22	68	55
<b>P6</b>	20,700	13,600	1.53	85	56
<b>P7</b>	6,000	4,650	1.29	29	22

## 2.2. Photophysical properties

The room-temperature optical absorption and emission spectra of **P1-P7** were measured in  $10^{-5}$  M  $\text{CH}_2\text{Cl}_2$  solution and the results are given in **Figures 1/2** and **Table 2**.

The absorption spectra of all seven polymers exhibit two absorption bands between 225-325 nm and 360-550 nm (**Figure 1**). The former can be assigned to  $\pi \rightarrow \pi^*$  electronic transitions on the chromophores (Soret bands) while the latter can be attributed to intra-molecular charge transfer (ICT) from the donor to the acceptor moieties (Q bands).<sup>28</sup> The measurements clearly highlight the sensitivity of the ICT band to the organic spacers. When an alkynyl linker is connected to a strong electron-donating moiety such as PTZ it acts as an electron acceptor, giving rise to donor-acceptor (D-A) interactions, and these can be reinforced

by connecting an electron-accepting moiety to the PTZ *via* the alkynyl linker. It has been shown that the D-A interactions are more prominent in organic polymers than in related metallopolymers.<sup>11</sup>

The trends in the absorption profiles can be understood by considering the electron withdrawing nature and conjugation length of the acceptor spacers connected to the donor PTZ. It is well established that fluorinated aryl, 2,1,3-benzothiadiazole, and 2,3-diphenylthieno[3,4-*b*]pyrazine have strong electron-withdrawing ability<sup>29-31</sup> and their electron-accepting strength varies in the order of tetrafluoro phenylene < 2,1,3-benzothiadiazole < 2,3-diphenylthieno[3,4-*b*]pyrazine. We found the same trend in the present systems, with the optical band gap ( $E_{g,opt}$ ) of the co-poly-ynes increasing in the order of **P4** (1.92 eV) < **P1** (2.15 eV) < **P3** (2.57 eV). **P2**, **P5** and **P7** all have S-containing five-membered heterocyclic spacers but exhibit different  $E_{g,opt}$  due to differences in conjugation length. One of us has previously demonstrated that fused thiophenes are less conjugated while bithiophenes are more so due to different numbers of C=C bonds.<sup>32</sup> The same holds true for the PTZ polymers reported in this work, with the  $E_{g,opt}$  falling in the order **P5** (2.51 eV) < **P7** (2.60 eV) ~ **P2** (2.63 eV). Comparing both sets of co-poly-ynes, we conclude that the 2,1,3-benzothiadiazole and thieno[3,2-*b*]thiophene spacers induce the strongest D-A interactions when connected to PTZ, followed by the tetrafluorophenyl and S-based heterocycles.<sup>33</sup>

**Table 2** Optical absorption maxima, optical bandgaps  $E_{g,opt}$ , and emission maxima, quantum yields and Stokes shifts of the co-poly-ynes **P1-P7**. All measurements were performed at room temperature in  $10^{-5}$  M  $\text{CH}_2\text{Cl}_2$  solution. Quantum yields are were measured relative to Rhodamine 6G (R6G).

	Absorption		Emission			
	$\lambda$ (nm) ( $\epsilon \times 10^4 \text{ mol}^{-1} \text{ cm}^{-1}$ )	Optical band gap $E_{g,opt}$ (eV)	$\lambda_{ex}$ (nm)	$\lambda_{em}$ (nm)	$\phi_F$ (%)	Stokes shift ( $\text{cm}^{-1}$ )
<b>P1</b>	487 (10.0), 354 (8.2), 316 (15.2), 255 (13.5)	2.15	-	N/A <sup>a</sup>	-	-
<b>P2</b>	420 (4.9), 324 (4.4), 299 (6.6), 230(14.0)	2.63	420	512	29.0	4278
<b>P3</b>	425(10.3), 304(7.9), 237(8.1)	2.57	416	556	17.0	5544
<b>P4</b>	545 (10.6), 379 (18.1) 335 (22.9), 279 (21.0)	1.92	-	N/A <sup>a</sup>	-	-
<b>P5</b>	429 (13.8), 356 (8.4), 288 (8.4), 238(8.3)	2.51	418	534	14.0	4583
<b>P6</b>	416 (5.8), 319 (6.8), 298 (9.3), 229(7.6)	2.62	408	509	41.0	4392
<b>P7</b>	419 (10.2), 327 (10.0), 291 (8.4), 236 (7.7)	2.60	407	520	13.0	4635

<sup>a</sup>**P1** and **P4** did not show detectable emission at room temperature.

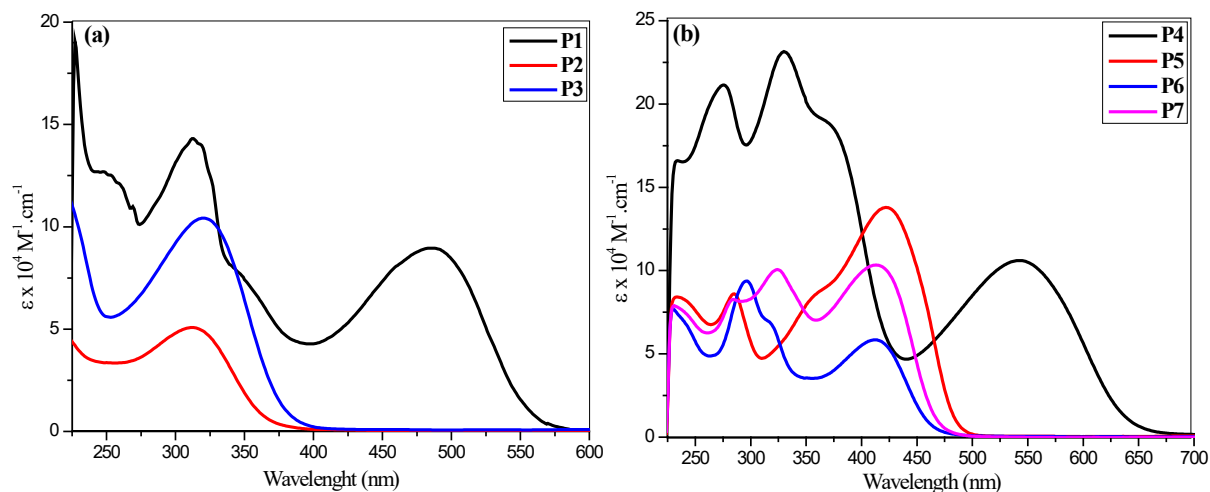


**Figure 1** Room temperature optical absorption spectra of the organic co-poly-yne (a) **P1 – P3** and (b) **P4 – P7** measured in  $10^{-5}$  M  $\text{CH}_2\text{Cl}_2$  solution.

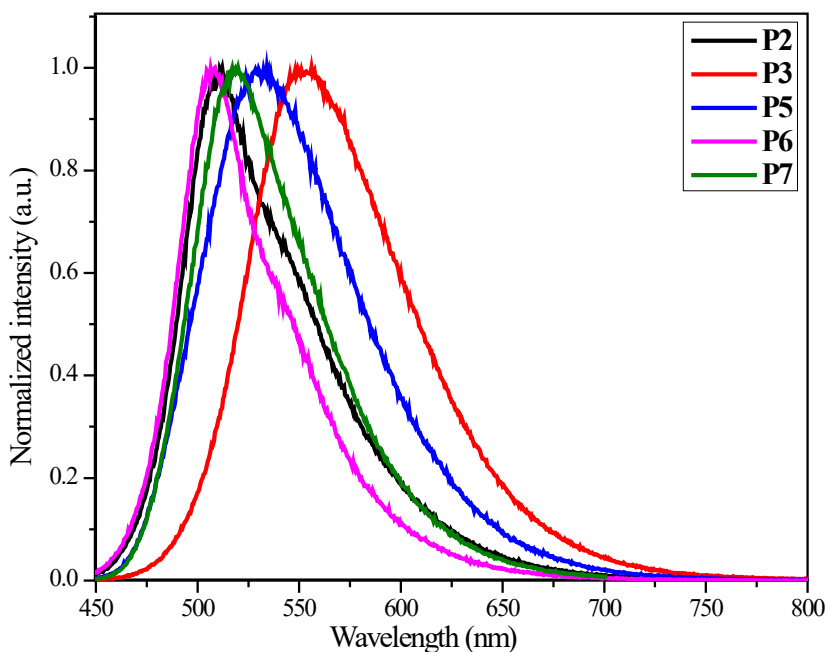


**Figure 2** Room temperature fluorescence emission spectra of the organic co-poly-yne **P2, P3, P5 – P7** in  $10^{-5}$  M  $\text{CH}_2\text{Cl}_2$  solution collected at the excitation wavelengths listed in **Table 2**.

**Figure 2** compares the room-temperature emission spectra of the organic co-poly-yne. With the exception of **P1** and **P4**, the co-poly-yne show a single fluorescence band between 450-600 nm which we assigned to the  $S_1$  singlet excited state. Large Stokes shifts of  $4278\text{-}5544\text{ cm}^{-1}$  (**Table 2**) can be attributed to structural changes occurring in this state, with the bent ground-state structure becoming more planar in on the  $S_1$  potential-energy surface.<sup>34</sup> The nature of the acceptor spacer group can be seen to have a substantial impact on the emission profile, with the emission maxima ( $\lambda_{em}$ ) varying in the order **P3 > P5 >**

**P7** > **P2** > **P6**. As for the absorption spectra, the emission spectrum of **P6** was found to be the most blue-shifted, which could be attributed to the biphenyl moieties adopting a more twisted conformation. The quantum yields  $\phi_F$  of the polymers determined relative to the rhodamine 6G dye (R6G; **Table 2**) highlight the crucial role of the extent of the conjugation, with **P6** and **P7** having the highest and lowest values of  $\phi_F$  = 41 and 13 % respectively.

### 2.3. Computational modelling

To better understand the optical spectroscopy, we performed quantum-chemical calculations using hybrid density-functional theory (DFT) on the precursor PTZ moiety **4** and a set of model compounds **M1-M7** approximating **P1-P7**. **M1-M7** each comprise a chain of three PTZ and two spacer moieties, with the terminal alkyne groups capped by methyl substituents. Images and coordinates of the optimized structures of **4** and **M1-M7** can be found in **Figures S1-S8** and **Listings S1-S8** (Supporting Information).

**Table 3** Calculated frontier highest-occupied and lowest-unoccupied orbital (HOMO/LUMO) energies and bandgaps of the precursor PTZ moiety **4** and the model compounds **M1-M7**. The orbital energies are expressed as a difference in energy  $\Delta E_{\text{HOMO}}/\Delta E_{\text{LUMO}}$  relative to **4**.

	$\Delta E_{\text{HOMO}}$ [Ha]	$\Delta E_{\text{LUMO}}$ [Ha]	$E_g$ (eV)
<b>4</b>	0	0	6.25
<b>M1</b>	0.285	-1.588	4.38
<b>M2</b>	0.319	-0.934	5.00
<b>M3</b>	0.132	-1.105	5.01
<b>M4</b>	0.489	-1.583	4.18
<b>M5</b>	0.326	-0.966	4.96
<b>M6</b>	0.229	-0.651	5.37
<b>M7</b>	0.355	-0.809	5.09

The calculated HOMO-LUMO bandgaps  $E_g$  are shown in **Table 3**, and isosurface plots of the frontier orbitals are shown in **Figures S9-S16** (Supporting Information). Qualitatively, the bandgaps fall into a rough grouping of **4** > **M2, M3, M5, M6, M7** > **M1, M4**, where **4** has the widest  $E_g$  of 6.25 eV, five of the model compounds have bandgaps in the range of 4.96-5.37 eV, and **M1** and **M4** have the narrowest  $E_g$  of 4.38 and 4.18 eV respectively. The bandgaps in the model compounds are thus reduced by 16-33 % relative to the PTZ precursor **4**. Inspection of the frontier orbitals shows that **M1-M7** have heavily delocalized HOMOs that extend across all three PTZ moieties and both spacer groups. On the other hand, the LUMOs, while also very delocalized, do not extend completely across the two terminal PTZ units. Interestingly, the nodal pattern in the HOMO and LUMO of **4** are reflected in the corresponding frontier orbitals of the model compounds, which may be taken to suggest that the frontier orbitals of the model compounds consist, to first approximation, of combinations of the frontier orbitals on the subunits.



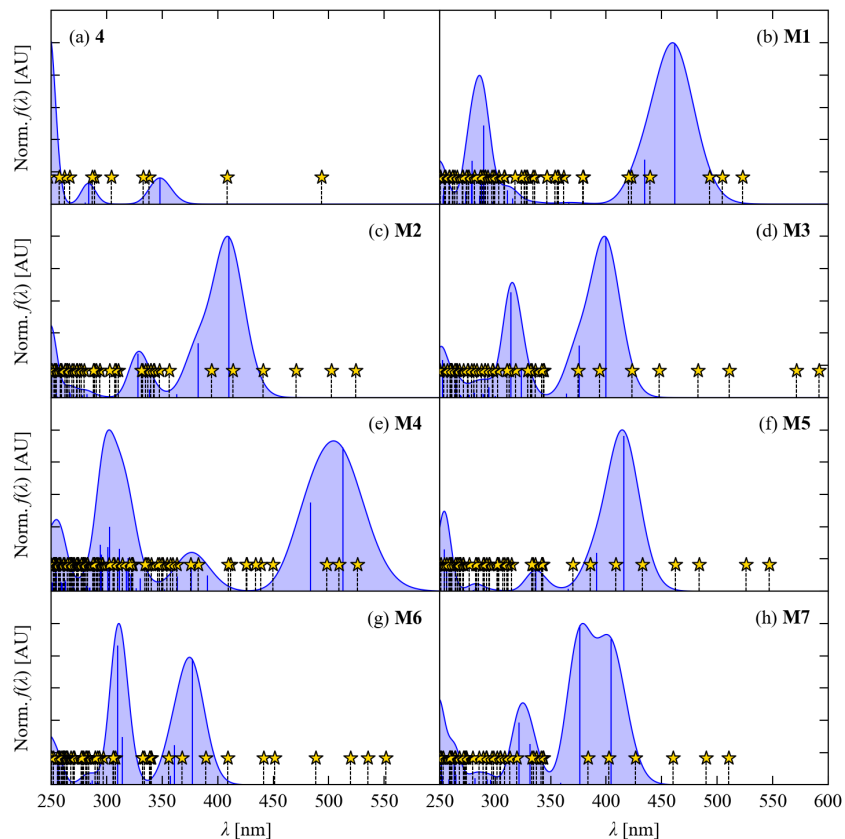


**Figure 3** Simulated absorption spectra of the precursor PTZ moiety **4** (a) and the model compounds **M1-M7** (b)-(h), obtained from TD-DFT calculations. The spectra shown as shaded blue curves were calculated based on the energies and dipole oscillator strengths of the spin-allowed (singlet) transitions and a nominal Gaussian broadening with a width  $\sigma = 0.1$  eV. The positions and relative intensities of the individual transitions are marked with vertical blue lines. The energies of spin-forbidden (triplet) states are marked as dashed lines with gold stars.

Taking the orbital energies of **4** as a reference point, we find that the HOMOs of the model compounds are raised in energy (i.e. destabilized) by 0.1-0.5 eV while the LUMOs are lowered in energy (i.e. stabilized) by 0.6-1.6 eV. While both will ultimately have an effect on narrowing the bandgap, these numbers suggest that the stabilization of the LUMO in the model compounds has the largest impact on the bandgap. Indeed, the LUMOs of **M1** and **M4** are calculated to be  $\sim 0.5$  eV lower in energy than any of the other model compounds relative to **4**, which goes some way to accounting for the narrower bandgaps of these two systems.

The calculated bandgaps are  $1.9\text{-}2.2 \times$  larger than the measured optical bandgaps in **Table 2** and are also larger than the electrochemical bandgaps presented in the following section (see **Table 6**). Furthermore, they are also considerably larger than the lowest-energy singlet (spin-allowed) optical excitations predicted from time-dependent DFT (TD-DFT) calculations (**Table 4**). This discrepancy may be

ascribed to fundamental limitations of ground-state Kohn-Sham DFT,<sup>35</sup> and/or to the truncated model compounds being an approximation to the extended electronic structure of the polymers. The  $E_g$  nevertheless correctly predict that **P1** and **P4** have the lowest  $E_{g,opt}$  while the other systems fall into a similar range, and the 1.2 eV range between **M1-M7** is proportionally larger than the 0.71 range between the measured  $E_{g,opt}$  of **P1-P7**.

Simulated absorption spectra (**Figure 3**) reproduce the main qualitative trends in the measured spectra in **Figure 1**, and, in particular, correctly predict the longer-wavelength absorption maxima in **P1** and **P4** and the similar positions of the maxima in the spectra of the other five co-poly-ynes. The simulated spectrum of **M7** (**Figure 3h**) predicts a split long-wavelength band comprised of two almost equally intense transitions - while this splitting is not clearly visible in the measured spectrum of **P7** in **Figure 1**, the absorption maximum does have an asymmetric band shape, and the discrepancy may therefore be due simply to our choice of broadening. Quantitatively the absorption maxima are blue shifted by 10-40 nm relative to the measurements, which may be ascribed to solution effects and/or the extended conjugation in the co-poly-ynes compared to the model compounds. While the former could be tested and corrected by performing the calculations using an implicit-solvent model, we opted not to do this in the present calculations as we doubt that a single solvent environment would capture the range of environments in the solution measurements and test devices investigated in this work.

**Table 4** Characterization of the brightest spin-allowed (singlet) transitions in the precursor PTZ moiety **4** and the model compounds **M1-M7**. The states are labelled such that  $S_0$  is the ground state and  $S_1$  and  $S_2$  the first and second excited states respectively. For each state, the energy and wavelength are given in eV and nm together with the dipole oscillator strength  $f$ .

	State	$E$ (eV)	$\lambda$ (nm)	$f$
<b>4</b>	$S_1$	3.56	348	0.135
<b>M1</b>	$S_1$	2.68	462	2.712
<b>M2</b>	$S_1$	3.03	410	3.681
<b>M3</b>	$S_1$	3.10	400	2.747
<b>M4</b>	$S_1$	2.42	513	1.660
	$S_2$	2.56	484	1.022
<b>M5</b>	$S_1$	2.98	416	4.161
<b>M6</b>	$S_1$	3.29	377	2.599
<b>M7</b>	$S_1$	3.06	405	1.772
	$S_2$	3.29	376	1.941

**Table 4** lists the brightest 1-2 spin-allowed (singlet) transitions giving rise to the longest-wavelength absorption peaks in each of the simulated spectra. A breakdown of each of the transitions listed in **Table 4** into component transitions between pairs of occupied and virtual states is given in **Tables S1-S10** (Supporting Information). This data clearly shows that the transitions in the model compounds are significantly red shifted compared to **4** and show a 5-30  $\times$  enhancement in the dipole oscillator strengths. The  $S_1$  state in **4** can be assigned as a “pure” HOMO  $\rightarrow$  LUMO transition. With the exception of the  $S_2$  states in **M4** and **M7**, the HOMO  $\rightarrow$  LUMO transition is the largest component of the brightest transitions in

the model compounds, but only accounts for ~45-60 % of the electron-density redistribution on the sum of squared coefficients. In the  $S_2$  state of **M4**, the HOMO  $\rightarrow$  LUMO + 1 and HOMO - 1  $\rightarrow$  LUMO account for 51 and 34 % of the sum of squared coefficients, respectively. In the  $S_2$  state of **M7**, the dominant components are again the HOMO  $\rightarrow$  LUMO + 1 and HOMO - 1  $\rightarrow$  LUMO transitions, which account for 38 and 32 % of the sum of squared coefficients.

To further investigate the nature of the transitions, we used the method of natural transition orbitals (NTOs)<sup>36</sup> to visualize the occupied particle and virtual hole states associated with each of the transitions listed in **Table 4 (Figures S17-S26)**. For the precursor PTZ moiety **4**, the NTO analysis yields a single pair of NTOs corresponding to the HOMO and LUMO and the  $S_1$  state can be assigned as a  $\pi \rightarrow \pi^*$  transition. For the model compounds, the NTO analysis yields two pairs of NTOs with > 10 % contribution to the transition. In most cases, both NTOs closely resemble the delocalized HOMOs and LUMOs, albeit with reduced contributions from the terminal PTZ units. The NTO analyses therefore show that the transitions involve a redistribution of the electron density across large parts of the molecules, but it is difficult to assign them definitively as ICT or  $\pi \rightarrow \pi^*$ . Two notable exceptions to this pattern are the  $S_1$  state in **M5**, for which the electron density in the largest contributing transition is concentrated around the central PTZ moiety, and the  $S_2$  state in **M7**, which consists of two component transitions between states partly localized on the two halves of the molecule.

Extrapolating from the model compounds to the polymers, one might anticipate that the extended structure would produce a large number of states that are closely spaced in energy (i.e. a “bandwidth”), which would in turn produce a high density of optically-bright transitions. This supports the hypothesis that, by tuning the bandgap through suitable selection of the spacer group, it should be possible to engineer copolyynes with strong visible absorption, as we demonstrate in this work.

**Table 5** Energies and wavelengths of the lowest-lying spin-forbidden (triplet) transition  $T_1$  in each of the precursor PTZ moiety **4** and the model compounds **M1-M7**.

	<i>E</i> (eV)	$\lambda$ (nm)
<b>4</b>	2.51	494
<b>M1</b>	1.41	882
<b>M2</b>	1.83	676
<b>M3</b>	2.09	592
<b>M4</b>	1.03	1206
<b>M5</b>	1.74	712
<b>M6</b>	2.25	551
<b>M7</b>	1.88	659

Finally, we note that the simulated spectra in **Figure 3** indicate the presence of spin-forbidden (triplet) states. The energies and wavelengths of the lowest-lying  $T_1$  states are collected in **Table 5**. The  $T_1$  states invariably have lower energies than the  $S_1$  states, and for some of the model compounds even extend into the infrared part of the spectrum. However, given their nature, it is not clear how accessible these states would be and therefore what role they would play in the optical properties. Discerning this would require further, somewhat involved, excited-state calculations that are beyond the scope of this study.

## 2.4. Electrochemical properties

Cyclic voltammetry (CV) measurements were performed on the polymer-modified interfaces in 0.1 M Bu<sub>4</sub>NPF<sub>6</sub>/CH<sub>3</sub>CN solution using 1.0 mM ferrocene as an internal reference to determine and compare the redox potentials of the co-poly-ynes. All seven co-poly-ynes exhibited quasi-reversible oxidation and reduction features (**Figure 4, Table 6**). The multiple pseudo-reversible oxidations observed for the co-poly-ynes are similar to other reports on oligomers,<sup>37</sup> co-polymers<sup>38</sup> and homopolymers<sup>39</sup> of PTZ. **P5** and **P6** show two oxidation peaks at the anodic peak potentials  $E_{pa}^{ox} = 0.63/0.42$  and  $0.52/0.39$  V vs. Fc<sup>+0</sup>, respectively, which were tentatively ascribed to the formation of radical cation and dication species. The first oxidation of the phenothiazine moiety leads to the formation of a radical cation species at the nitrogen center, which is converted to the dication species by further oxidation of the electron pair at the sulfur atom. Upon scanning in the negative region, all the co-poly-ynes exhibited electron acceptor dependent reduction waves (**Figure 4**). The measured redox potentials were also used to determine the energy levels of the frontier orbitals (i.e. the HOMO and LUMO) according to:<sup>40</sup>

$$E_{LUMO} = [(E_{red^-} - E_{1/2}(\text{ferrocene})) + 4.8] \text{ eV}$$
$$E_{HOMO} = [(E_{ox^-} - E_{1/2}(\text{ferrocene})) + 4.8] \text{ eV}$$

In current studies, ferrocene was used as an internal standard (see Figure S27). Two peaks at 0.37 and 0.44 V vs. Ag/AgCl were observed, hence the  $E_{1/2}(\text{ferrocene})$  is equal to approx. 0.41 V vs. Ag/AgCl and employed as potential reference (see Figure 4). The calculated HOMO and LUMO levels are presented in **Table 6** and give electrochemical band gaps  $E_{g,ele}$  in the range of 1.80-2.09 eV. The electrochemical results are in good agreement with optical spectroscopy and theoretical calculations. These are notably smaller than the measured optical band gaps, but this is expected as they refer to distinct processes - the optical bandgaps correspond to the energies required to effect a “vertical” excitation or to form a bound exciton, whereas the electrochemical (transport) band gaps are the energies required to form free carriers.<sup>41, 42</sup>

The redox behavior of the co-poly-ynes suggest that p- and n-type doping of these materials to form conducting states would be feasible, so the systems could be used as electrochemically amphoteric push-pull chromophores that can accept or release electrons at relatively low voltages. They could also be utilized for applications in organic light-emitting diodes (OLEDs) or organic field-effect transistors as functional hole- and electron-transport layers. Additionally, the highly fluorescent co-poly-ynes **P2-P3** and **P5-P7** could also potentially serve as redox-switchable emitters in OLED devices. We explore some of these points further in the following subsection.

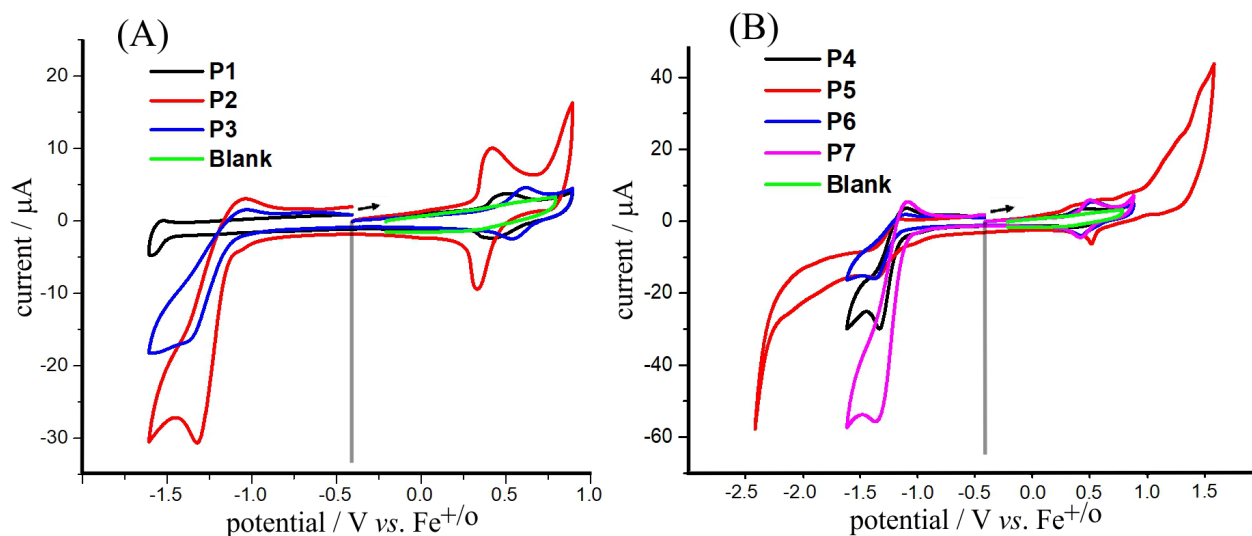


**Figure 4.** Cyclic voltammograms of polymer-modified interfaces with (A) **P1 – P3** and (B) **P4 – P7** in 0.1 M Bu<sub>4</sub>NPF<sub>6</sub>/CH<sub>3</sub>CN solution, at a scan rate of 100 mV/s at positive and negative potentials.

**Table 6** Electrochemical redox properties of the co-poly-ynes **P1 – P7** in 0.1 M Bu<sub>4</sub>NPF<sub>6</sub>/CH<sub>3</sub>CN solution using ferrocene as an internal reference potential: oxidation and reduction peak potentials  $E_{\text{peak}}^{\text{ox}}/E_{\text{peak}}^{\text{red}}$ , HOMO and LUMO energy levels are used to calculate electrochemical bandgap  $E_{\text{g,ele}}$ .

co-poly-ynes	$E_{\text{peak}}^{\text{ox}}$ (V vs. Fc <sup>+/0</sup> ) / $E_{\text{peak}}^{\text{red}}$ (V vs. Fc <sup>+/0</sup> )	$E_{\text{HOMO}}$ (eV)	$E_{\text{LUMO}}$ (eV)	$E_{\text{g,ele}}$ (eV)
P1	0.40 / -1.59	5.20	3.21	1.99
P2	0.51 / -1.31	5.31	3.49	1.82
P3	0.52 / -1.36	5.32	3.44	1.88
P4	0.47 / -1.32	5.27	3.48	1.79
P5	0.59 / -1.37	5.39	3.44	1.95
P6	0.63 / -1.34	5.43	3.46	1.97
P7	0.64 / -1.33	5.44	3.47	1.97

## 2.5 Electroluminescence in polymer light-emitting diodes (PLEDs)

The strong photoluminescence (PL) efficiency of the polymers in solution suggests potential applications in polymer light-emitting diodes (PLEDs).<sup>43-45</sup>

We therefore took **P7** as a base to optimize electroluminescent devices with single emissive layers, comprising stacks of ITO/PEDOT:PSS (40 nm)/TFB (20 nm)/**P7**:PVK (30 nm)/TPBi (20 nm)/LiF (1 nm)/Al (100 nm). (ITO - indium tin oxide; PEDOT:PSS - poly(3,4-ethylenedioxythiophene)/ poly(styrenesulfonate); TFB - poly(9,9-dioctylfluorene-co-N-(4-butylphenyl)diphenylamine); PVK - poly(9-vinylcarbazole); TPBi - benzimidazol-2-yl)benzene.) Here, PEDOT:PSS and TFB serve as the hole-injection and hole-transporting materials, respectively, TPBi serves as both an electron-transporting and a hole-blocking material, and LiF

serves to enhance the electron injection. The **P7**:PVK layer was spin-coated from a chlorobenzene solution with a controlled ratio and film thickness.

In order to obtain high-performance devices, different doping concentrations of **P7** in the PVK host material were tested. The electroluminescence spectra and current density-voltage-luminance (*J-V-L*), current efficiency-luminance (*CE-L*), power efficiency-luminance (*PE-L*) and external quantum efficiency-luminance (*EQE-L*) characteristics of the devices are shown in **Figure S29-S32** (Supporting Information). These tests indicated that a 30 nm **P7**:PVK layer containing 10 wt. % of the co-poly-yne exhibited the best performance, with a peak emission wavelength of 518 nm, a maximum current efficiency of 3.34 cd A<sup>-1</sup>, a maximum power efficiency of 3.16 lm W<sup>-1</sup>, and a maximum external quantum efficiency (EQE) of 1.21 %. In this device geometry, a brightness of 1.1 × 10<sup>4</sup> cd m<sup>-2</sup> was obtained, which is higher than reported for other poly-yne based PLEDs.<sup>46, 47</sup> The results are also comparable to or higher than other reported PTZ-based OLED materials.<sup>45, 48</sup> We also noted a clear emission shoulder between 400-500 nm which decreased in intensity with increasing doping concentration, and which may therefore be emission from the PVK host material.

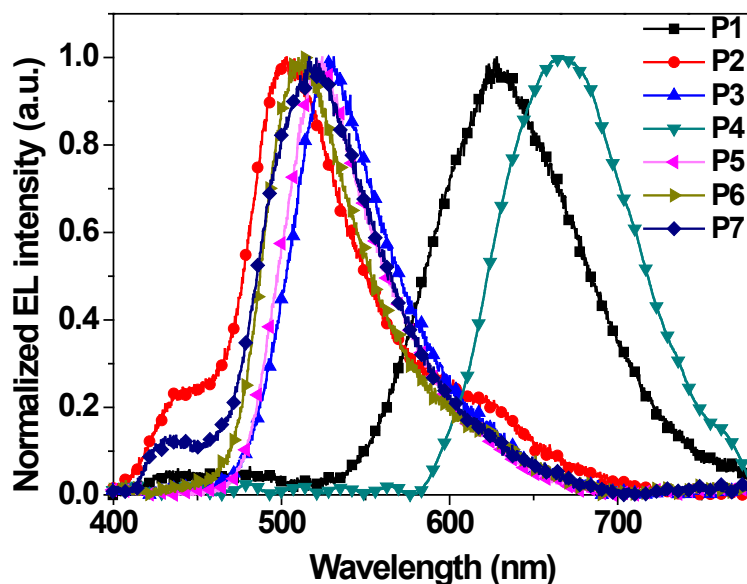


**Figure 5** Electroluminescence (EL) emission spectra of polymer light-emitting diode (PLED) devices based on the organic co-poly-ynes **P1 – P7**.

We next proceeded to fabricate devices based on **P1-P6** using the optimal configuration identified for **P7**. Electroluminescent devices based on these polymers exhibited emission ranging from green to deep red and near-infrared (NIR) (**Figure 5**). The *J-V-L* curves of the devices are compared in **Figure S33** (Supporting Information). The maximum emission wavelengths and corresponding Commission Internationale de L'Eclairage (CIE) coordinates and the turn-on voltages, maximum luminance, current and power efficiencies, and external quantum efficiencies of the devices are compared in **Table 7**. **Figure 6**

compares the CE-L, PE-L and EQE-L of the devices based on **P1**, **P3**, **P5**, and **P7**, and the corresponding measurements for devices based on **P2**, **P4**, and **P6** are shown in **Figure S34** (Supporting Information).

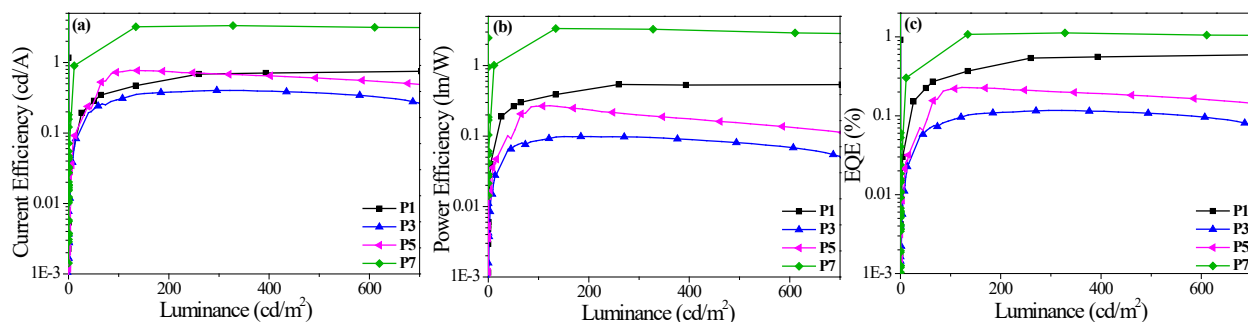


**Figure 6** Current efficiency-luminance (CE-L) (a), power efficiency-luminance (PE-L) (b), and external quantum efficiency-luminance (EQE-L) (c) curves for polymer light-emitting diode (PLED) devices based on the organic co-poly-ynes **P1**, **P3**, **P5**, and **P7**.

**Table 7** Electroluminescence properties of polymer light-emitting diode (PLED) devices based on the organic co-poly-ynes **P1-P7**: peak electroluminescent emission wavelength  $\lambda_{EL}$  and corresponding CIE color coordinates, maximum luminance  $L_{max}$ , turn-on voltage  $V_{on}$ , maximum current and power efficiency (CE/PE), and maximum external quantum efficiency (EQE).

	$\lambda_{EL}$ (nm)	CIE	$L_{max}$ (cd m <sup>-2</sup> )	$V_{on}$ (V)	CE (cd A <sup>-1</sup> )	PE (lm W <sup>-1</sup> )	EQE (%)
<b>P1</b>	627	(0.59, 0.37)	3160	2.9	0.79	0.52	0.60
<b>P2</b>	503	(0.26, 0.44)	168	5.0	0.17	0.06	0.07
<b>P3</b>	528	(0.32, 0.60)	700	6.2	0.39	0.10	0.18
<b>P4</b>	667	(0.64, 0.29)	45	7.0	0.03	0.01	0.06
<b>P5</b>	525	(0.31, 0.61)	619	4.8	0.77	0.27	0.22
<b>P6</b>	511	(0.28, 0.57)	539	6.0	0.27	0.08	0.09
<b>P7</b>	518	(0.28, 0.52)	10776	2.7	3.34	3.16	1.21

## 2.5. Power-conversion efficiency in polymer solar cells

Polymer solar cells (PSCs) using the co-poly-ynes with relatively high absorption coefficients (**P5/P7**) and with more red-shifted absorption profiles (**P1/P4**) as electron donors and phenyl-C61-butyric acid methyl ester (PCBM) as an electron acceptor were fabricated and characterized (**Table 8**). ITO spin-coated with PEDOT:PSS was used as the hole-collecting electrode, while the electron-collecting electrode was formed from Al/Ca.

**Figure 7** shows the  $J$ - $V$  curves of solar cells with 1:1 w/w donor and acceptor active layers under simulated AM1.5 solar irradiation. The power-conversion efficiency (PCE) of the devices increases in the order **P5** < **P4** < **P7** < **P1**. The best-performing cell is that with **P1** as an electron donor, which has an open-circuit voltage ( $V_{oc}$ ) of 0.46 V, a short-circuit current density ( $J_{sc}$ ) of 1.94 mA cm<sup>-2</sup>, and an electrical fill factor (FF) of 27.17 %, resulting in an overall PCE of 0.24 %. This device shows a markedly better  $J_{sc}$  and PCE compared to devices based on the other co-poly-ynes in the same blend ratio. Efficient conversion depends

on both the absorption wavelength and the absorption coefficient, and the enhanced absorption coefficient of **P1**, obtained by increasing the co-poly-yne conjugation chain length with additional thienyl rings, suggests this represents an effective strategy for optimizing the co-poly-yne to improve the PSC performance. The requirement for a high absorption coefficient is also seen in the relative performance of **P5/P7** ( $\epsilon = 13.8 \times 10^4/10.2 \times 10^4 \text{ M}^{-1} \text{ cm}^{-1}$ ) and **P4/P1** ( $10.6 \times 10^4/10.0 \times 10^4 \text{ M}^{-1} \text{ cm}^{-1}$ ).

**Table 8** Device characteristics of polymer solar cells made with 1:1 blends of the co-poly-yne **P1**, **P4**, **P5** and **P7** and PCBM as the donor materials with the specified film thickness: short-circuit current density ( $J_{sc}$ ), open-circuit voltage ( $V_{oc}$ ), fill factor (FF), power-conversion efficiency (PCE), and integrated current from external quantum efficiency (EQE). The characteristics of a device using pure PCBM as a donor are shown for comparison.

Donor	Film thickness (nm)	$J_{sc}$ (mA/cm <sup>2</sup> )	$V_{oc}$ (mV)	FF (%)	PCE (%)	Integrated current (EQE) (mA/cm <sup>2</sup> )
<b>P1</b>	84	1.94	0.46	27.17	0.24	2.09
<b>P4</b>	90	0.56	0.51	25.92	0.07	0.70
<b>P5</b>	110	1.19	0.17	26.08	0.05	1.04
<b>P7</b>	72	0.76	0.43	29.69	0.10	1.18
<b>PCBM</b>	77	0.05	0.003	0	0	-

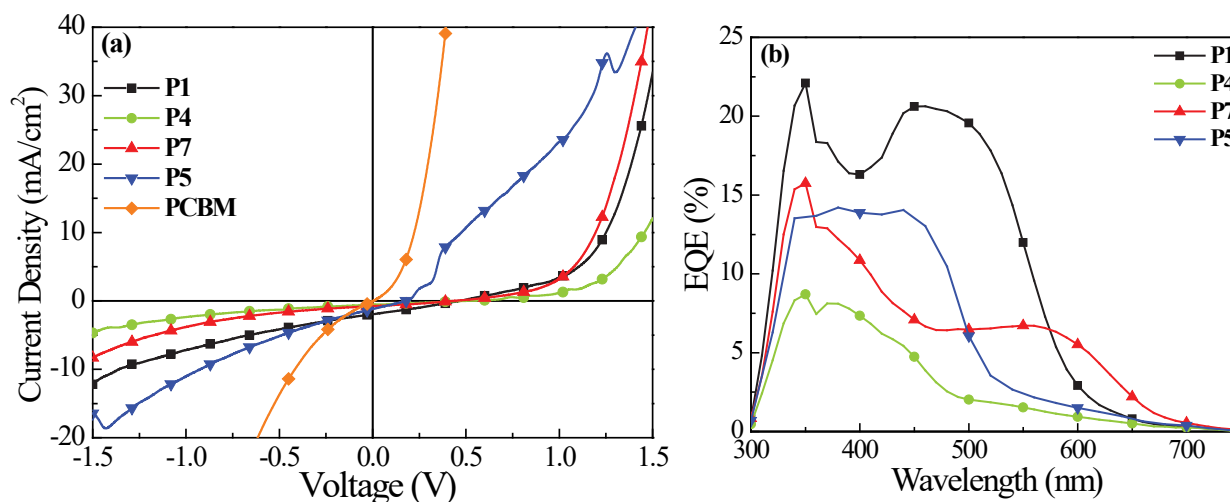


**Figure 7** (a) Current density-voltage ( $J$ - $V$ ) and (b) external quantum efficiency (EQE) curves for polymer solar cells made with 1:1 blends of the co-poly-yne **P1**, **P4**, **P5**, **P6** and **P7** and PCBM as donor materials. The  $J$ - $V$  curves also show measurements performed on a device using PCBM as a donor material for comparison.

The best-performing **P1** device was further optimized by varying the spin-coating rate from 600-1800 rpm (**Figure S35**, **Table S11**, Supporting Information), producing film thicknesses from 54-115 nm. We found that a speed of 1200 rpm, which produces a film of ca. 84 nm, gave the optimal device characteristics.

The relatively small electrochemical band gaps of **P1**, **P4**, **P5** and **P7** translate to low  $V_{oc}$  values of 0.46, 0.51, 0.43 and 0.17 V, respectively. Moreover, the LUMO level of the PCBM acceptor (-3.41 eV)<sup>12</sup> is



higher than the electrochemical LUMO levels of **P4** (-3.46 eV), **P5** (-3.44 eV) and **P7** (-3.46 eV), but lower than that of **P1** (-3.20 eV), which explains the low PCE of the devices based on **P4**, **P5** and **P7** (c.f. **Table 8**). The design of polymers for photovoltaic applications should therefore consider the optical bandgap, the absorption coefficient, the absolute positions of the energy levels, and optimizing the thickness of the blend films.

The fill factors are not particularly high in our devices because all processing, save for the PEDOT:PSS annealing and electrode deposition, and all measurements were performed in ambient air, which likely results in the formation of trap states. We therefore expect that the fill factors could be improved by fabricating and characterizing the devices under inert atmosphere. A more comprehensive study of charge transport and the influence of traps is therefore necessary to further improve the overall device performance. Nonetheless, these studies demonstrate that our approach of optimizing the spacer group in PTZ-based co-poly-ynes can potentially serve as a “bottom-up” strategy to designing high-performance PSCs.

### 3. Conclusions

We have synthesized and characterized a series of seven acetylide-functionalized phenothiazine-based organic co-poly-ynes. The synthetic procedure we presented affords the co-poly-ynes in moderate to high yields of 28-83 %, and the formation of the desired products was confirmed by spectroscopic characterization. GPC indicates molecular weights between 4,000-50,000 g mol<sup>-1</sup>, corresponding to degrees of polymerization between 13 and 213, and relatively narrow polydispersity indices of 1.12-1.78.

Optical absorption measurements reveal absorption coefficients on the order of 10<sup>5</sup> mol<sup>-1</sup> cm<sup>-1</sup> and optical bandgaps in the range of 1.92-2.63 eV. With the exception of **P1** and **P4**, the materials show emission in solution, with quantum yields in the range of 13-41 % relative to Rhodamine 6G. Quantum-chemical calculations on the precursor PTZ moiety **4** and model compounds **M1-M7** approximating **P1-P7** highlight the role of the spacer group and the extended conjugation in the co-poly-ynes on narrowing the bandgap, pushing the absorption into the visible region of the electromagnetic spectrum and enhancing the absorption coefficient. The HOMO and LUMO levels were derived from electrochemical measurements of the oxidation and reduction potentials in solution and found to be in the range of 5.26 to 5.44 eV and 3.20 to 3.49 eV, respectively, giving electrochemical band gaps between 1.80-2.09 eV.

Finally, we also assessed the performance of the co-poly-ynes in polymer light-emitting diode (PLED) and bulk heterojunction polymer solar cell (PSC) devices. **P7** exhibited the best PLED performance with a peak emission wavelength of 518 nm, maximum current efficiency of 3.34 cd A<sup>-1</sup>, maximum power efficiency of 3.16 lm W<sup>-1</sup>, and maximum external quantum efficiency of 1.21 %. **P1** and **P4**, which did not show emission in solution, were found to show electroluminescent emission at long wavelengths. PSCs fabricated using a 1:1 blend of PCM and **P1** exhibited a moderate power conversion efficiency of 0.24 %, which might be improved by fabricating and testing devices under inert atmosphere. The lower PCEs obtained using donors based on the other co-poly-ynes are likely attributable to the LUMO levels being lower than those of the PCBM acceptor (-3.41 eV).

In summary, we find that the extended conjugation in the co-poly-ynes result in strong absorption and emission in the visible region of the spectrum together with a range of electrochemical properties that make these materials suitable for a range of molecular electronic devices. This is confirmed by the demonstration of working PLED devices with green to deep red and near-infrared emission and a functional PSC device that operates with acceptable power-conversion efficiency, obtained without optimization, based on one of the polymers.

To the best of our knowledge, this is the first report of co-poly-ynes incorporating PTZ as the donor molecule for PLED and PSC devices, and our results not only provide a better understanding of the relationship between the structures of the donor-acceptor systems and their optoelectronic properties, but also highlight a flexible route to designing novel PTZ-based co-poly-ynes for organic electronics. Overall, our results shed valuable light on the relationships between the molecular and electronic structure in this family of materials, demonstrating that the optoelectronic properties can be tuned by careful selection of the spacer group for solid-state lighting and solar-energy harvesting.

## 4. Experimental Section

### 4.1. General Procedures

All reactions were conducted under dry Ar using standard Schlenk techniques. Unless stated otherwise, all chemicals were obtained from Sigma-Aldrich and used as received. NMR spectra were recorded in CDCl<sub>3</sub> using Bruker WM-250 and AM-400 spectrometers and a Bruker Avance III HD 700 MHz spectrometer equipped with 5 mm TCI H/C/N cryoprobe. The <sup>1</sup>H and <sup>13</sup>C NMR spectra were referenced to solvent resonances. IR spectra were recorded in attenuated total reflectance (ATR) mode on Diamond using a Cary 630 FT-IR spectrometer. UV/vis spectra were recorded using a Shimadzu UV-2450 spectrometer. Electrospray ionization (ESI) mass spectra were recorded using a Kratos MS 890 spectrometer. Microanalyses were performed at the Department of Chemistry, Sultan Qaboos University. Preparative thin layer chromatography was carried out on commercial Merck plates with a 0.25 mm silica layer. Column chromatography was performed using Kieselgel 60 silica gel (230–400 mesh).

### 4.2. Synthesis of PTZ-based ligand

#### 4.2.1. 10-(2-Ethylhexyl)-10H-phenothiazine (1)

A reaction mixture of 2-ethylhexyl bromide (16.58 g, 0.085 mol), phenothiazine (10 g, 0.050 mol) and potassium *t*-butoxide (5.72 g, 0.051 mol) in tetrahydrofuran (THF, 200 ml) was refluxed overnight. After completion of the reaction, removal of the solvent *in vacuo* followed by purification using column chromatography gave the title compound as a colorless viscous liquid (14.28 g, 90%). The resulting liquid was further purified by column chromatography (9.53 g, 67 %). <sup>1</sup>H NMR (700 MHz, CDCl<sub>3</sub>): δ<sub>H</sub>/ppm 7.05-7.02 (m, 4H), 6.81-6.77 (m, 4H), 3.61 (d, 2H), 1.84 (m, 1H), 1.37-1.22 (m, 1H), 1.18-1.16 (b, 6H), 0.82-0.75 (m, 6H). <sup>13</sup>C NMR (176 MHz, CDCl<sub>3</sub>): δ<sub>C</sub>/ppm 145.83, 127.64, 127.17, 125.90, 122.44, 116.00 (aromatic), 51.12 (NCH<sub>2</sub>), 35.85 (alkyl CH), 30.82, 28.67, 24.13, 23.17 (alkyl CH<sub>2</sub>), 14.13, 10.60 (alkyl CH<sub>3</sub>). Anal. calc.

for C<sub>20</sub>H<sub>25</sub>SN: C – 77.12, H – 8.09; N – 4.50 %; found C – 76.69, H – 8.12, N – 4.48 %. ESI-MS: *m/z* 312.3 [M + 1]<sup>+</sup>.

#### 4.2.2.3,7-Dibromo-10-(2-ethylhexyl)-10H-phenothiazine (2)

To a solution of (*N*-ethylhexylphenothiazine) (5.00 g, 0.016 mol) in DMF (50 mL) was added 2.2 eq. of *N*-bromosuccinimide (17.3 g, 0.97 mol) in portions at room temperature, and the reaction mixture was stirred overnight. After reaction completion, water (100 mL) was added to the reaction mixture followed by saturated aqueous sodium thiosulfate (20 mL), and the organic product was extracted with hexane (2 × 300 mL). The combined organic layer was dried over anhydrous MgSO<sub>4</sub>. The solvent was removed under reduced pressure yielding a pale-yellow liquid (5.00 g, 69 %). <sup>1</sup>H NMR (700 MHz, CDCl<sub>3</sub>): δ<sub>H</sub>/ppm 7.11-7.09 (dd, 2H), 7.06 (d, 2H), 6.54 (d, 2H), 3.51-3.8 (m, 2H), 1.77-1.74 (q, 2H), 1.33-1.22 (m, 6H), 1.19-1.14 (d, 1H), 0.78-0.74 (m, 6H). <sup>13</sup>C NMR (176 MHz, CDCl<sub>3</sub>): δ<sub>C</sub>/ppm 144.35, 129.91, 129.65, 127.07, 116.95, 114.64 (aromatic), 51.05 (N-CH<sub>2</sub>), 35.69 (alkyl CH), 30.53, 28.44, 23.86, 22.99 (alkyl CH<sub>2</sub>), 14.01, 10.44 (alkyl CH<sub>3</sub>). Anal. calc. for C<sub>20</sub>H<sub>23</sub>Br<sub>2</sub>SN: C - 43.66, H - 2.88; N - 3.64 %; found C - 43.52, H - 2.88, N - 3.65 %. ESI-MS: *m/z* 470.1 [M + 1]<sup>+</sup>.

#### 4.2.3.3,7-Bis(trimethylsilylethynyl)-*N*-(2-ethylhexyl) 10H-phenothiazine (3)

To a solution of 3,7-dibromo-10-(2-ethylhexyl)-10H-phenothiazine **1** (1.00 g, 2.10 mmol) in *i*-Pr<sub>2</sub>NH/THF (70 mL, 1:4 v/v) under an Ar atmosphere was added catalytic amounts of CuI (10 mg), Pd(OAc)<sub>2</sub> (10 mg), and PPh<sub>3</sub> (52 mg). The solution was stirred for 30 min at room temperature, and then trimethylsilylethyne (0.61 mL, 4.28 mmol) was added under vigorous stirring. The reaction mixture was then refluxed overnight. The completion of the reaction was confirmed by preparative TLC and IR spectroscopy. After being cooled to room temperature, the mixture was filtered and concentrated under reduced pressure. The crude residue was dissolved in CH<sub>2</sub>Cl<sub>2</sub> and purified by silica column chromatography using a hexane/CH<sub>2</sub>Cl<sub>2</sub> (1:1 v/v) eluent to yield a yellowish viscous liquid (0.79 g, 75 %) IR (ATR, diamond): *v*/cm<sup>-1</sup> 2151 (C≡C). <sup>1</sup>H NMR (700 MHz, CDCl<sub>3</sub>): δ<sub>H</sub>/ppm 7.17-7.15 (m, 4H), 7.07 (s, 2H), 3.43-3.39 (m, 2H, NCH<sub>2</sub>), 1.66-1.62 (q, 2H), 1.20-1.09 (m, 1H), 1.05 (m, 6H, alkyl CH<sub>2</sub>), 0.70-0.63 (m, 6H, CH<sub>3</sub>), 0.09 (b, 18H, SiMe<sub>3</sub>). <sup>13</sup>C NMR (176 MHz, CDCl<sub>3</sub>): δ<sub>C</sub>/ppm 145.16, 130.99, 130.53, 124.95, 117.21, 115.63 (aromatic), 104.42, 93.77 (C≡C), 50.93 (NCH<sub>2</sub>), 35.70 (alkyl CH), 31.73, 28.70, 23.30, 22.97 (alkyl CH<sub>2</sub>), 13.86, 10.40 (alkyl CH<sub>3</sub>), 0.0 (SiMe<sub>3</sub>). ESI-MS: *m/z* 503.3 (M<sup>+</sup>). Anal. calc. for C<sub>30</sub>H<sub>41</sub>NSSi<sub>2</sub>: C - 71.51, H - 8.20, N - 2.78 %; found: C - 71.48, H - 8.19, N - 2.75 %.

#### 4.2.4.10-(2-Ethylhexyl)-3,7-diethynyl-10H-phenothiazine (4)

Bis(trimethylsilylethynyl) product **3** (0.60 g, 1.20 mmol) was proto-desilylated in THF/methanol (20 mL, 4:1, v/v) using aqueous KOH (0.13 g, 2.40 mmol). The reaction mixture was stirred at room temperature for 1 h, during which time preparative TLC and IR revealed that all the protected compound had been converted to the terminal alkyne ligand. The solvent was then removed, and the residue was dissolved in CH<sub>2</sub>Cl<sub>2</sub> and purified by column chromatography on silica using hexane/CH<sub>2</sub>Cl<sub>2</sub> (1:1, v/v) as eluent, to give the product as a yellow liquid (0.431 g, 100 %). IR (ATR, diamond): *v*/cm<sup>-1</sup> 2104 (C≡C), 3276 (C≡C-H). <sup>1</sup>H

NMR (700 MHz, CDCl<sub>3</sub>):  $\delta_{\text{H}}$ /ppm 7.21-7.20 (dd, 2H), 7.17 (s, 2H), 6.71 (d, 2H), 3.66-3.60 (m, 2H, NCH<sub>2</sub>), 2.97 (s, 2H, C-H), 1.38-1.25 (m, 1H), 1.17 (b, 8H, alkyl CH<sub>2</sub>), 0.79-0.77 (t, 6H, CH<sub>3</sub>), <sup>13</sup>C NMR (176 MHz, CDCl<sub>3</sub>):  $\delta_{\text{C}}$ /ppm 145.67, 131.38, 130.98, 125.22, 116.33, 115.73 (aromatic), 82.91 (C≡C), 51.17 (NCH<sub>2</sub>), 35.87 (alkyl CH), 30.56, 28.49, 23.89, 23.01 (alkyl CH<sub>2</sub>), 14.20, 10.43 (alkyl CH<sub>3</sub>). ESI-MS: *m/z* 359.2 (M<sup>+</sup>). Anal. calc. for C<sub>24</sub>H<sub>25</sub>NS: C - 80.18, H - 7.01, N - 8.92 %; found: C - 80.20, H - 6.99, N - 8.90 %.

### 4.3. Synthesis of PTZ-based co-poly-ynes

#### 4.3.1. Co-poly-yne P1

To a stirred mixture of **4** (0.150 g, 0.42 mmol) and 4,7-dibromo 2,1,3-benzothiadiazole (0.13 g, 0.42 mmol) in *i*Pr<sub>2</sub>NH (20 mL) and toluene (20 mL) was added (Ph<sub>3</sub>P)<sub>4</sub>Pd (25 mg, 0.02 mmol) and CuI (1 mg, 0.005 mmol) under argon. The reaction mixture was stirred for 30 mins at room temperature and then heated at 70 °C for ~30 h after which all volatile components were removed under reduced pressure. After removal of the solvent, a red solid was obtained, which was washed several times with methanol to give the final product (76.6 %). IR (ATR, diamond):  $\nu/\text{cm}^{-1}$  2087 (C≡C). <sup>1</sup>H NMR (700 MHz, CDCl<sub>3</sub>):  $\delta_{\text{H}}$ /ppm 7.76 (b, 2H, BTDH), 7.50-7.44 (m, 4H, PTZH), 6.90 (s, 2H, PTZH), 3.80-3.77 (dd, 2H, NCH<sub>2</sub>), 2.19 (s, 1H, CH), 1.59 (d, 2H, CH<sub>2</sub>) 1.30-1.27 (m, 6H, CH<sub>2</sub>), 0.92-0.89 (b, 6H, CH<sub>3</sub>). <sup>13</sup>C NMR (176 MHz, CDCl<sub>3</sub>):  $\delta_{\text{C}}$ /ppm 154.37, 145.82, 132.45, 132.14, 131.38, 130.79 (aromatic), 97.05, 85.78 (C≡C), 51.35 (NCH<sub>2</sub>), 36.01 (alkyl CH), 30.95, 28.51, 23.93, 23.01 (alkyl CH<sub>2</sub>), 14.02, 10.50 (alkyl CH<sub>3</sub>). Anal. calc. for C<sub>28</sub>H<sub>25</sub>N<sub>3</sub>S<sub>2</sub>: C - 71.61, H - 5.79, N - 8.95 %; found: C - 71.60, H - 5.65, N - 8.91 %. *M<sub>w</sub>* (g mol<sup>-1</sup>): 50,100, *M<sub>n</sub>*: 44,600, PDI: 1.12. Decomposition temp.: 170 °C.

#### 4.3.2. Co-poly-yne P2

A similar procedure used to synthesize **P1** was followed using **4** and 2,5-dibromothiopheno[3,2-*b*]thiophene to obtain a yellow solid (28%). IR (ATR, diamond):  $\nu/\text{cm}^{-1}$  2093 (C≡C). <sup>1</sup>H NMR (700 MHz, CDCl<sub>3</sub>):  $\delta_{\text{H}}$ /ppm 7.3 (m, 7H), 6.80-6.78 (d, 1H, PTZH), 3.51- 3.48 (b, 2H, NCH<sub>2</sub>), 2.17 (s, 1H, CH), 1.55 (s, 2H, CH<sub>2</sub>), 1.25 (b, 6H, CH<sub>2</sub>), 0.86 (b, 6H, CH<sub>3</sub>). <sup>13</sup>C NMR (176 MHz, CDCl<sub>3</sub>):  $\delta_{\text{C}}$ /ppm 144.43, 136.04, 131.84, 130.53, 129.74, 129.23, 128.59, 124.28, 115.82, 114.86 (aromatic), 93.24, 92.43, 81.46, 80.48 (C≡C), 47.98 (NCH<sub>2</sub>), 34.91 (alkyl CH), 30.95, 28.47, 23.01, 19.27 (alkyl CH<sub>2</sub>), 14.00, 10.44 (alkyl CH<sub>3</sub>). Anal. calc. for C<sub>28</sub>H<sub>27</sub>NS<sub>3</sub>: C - 70.99, H - 5.75, N - 2.96 %; observed: C - 70.92, H - 7.74, N - 2.94 %. *M<sub>w</sub>* (g mol<sup>-1</sup>): 6,000, *M<sub>n</sub>*: 4,500, PDI: 1.33. Decomposition temp.: 171 °C.

#### 4.3.3. Co-poly-yne P3

A similar procedure described above for **P1** was followed using **4** and 1,4-dibromo-2,3,5,6-tetrafluorobenzene to obtain a yellow solid (77.5 %). IR (ATR, diamond):  $\nu/\text{cm}^{-1}$  2090 (C≡C). <sup>1</sup>H NMR (700 MHz, CDCl<sub>3</sub>):  $\delta_{\text{H}}$ /ppm 7.40-7.30 (m, 4H, PTZH), 6.87-6.80 (s, 2H, PTZH), 3.77-3.72 (dd, 2H, NCH<sub>2</sub>), 2.17 (s, 1H, CH), 1.57 (s, 2H, CH<sub>2</sub>), 1.44-1.37 (m, 6H, CH<sub>2</sub>), 0.90-0.80 (b, 6H, CH<sub>3</sub>). <sup>13</sup>C NMR (176 MHz, CDCl<sub>3</sub>):  $\delta_{\text{C}}$ /ppm 146.27, 131.49, 131.22, 130.77, 125.40 (aromatic), 115.99 (C≡C), 51.25 (NCH<sub>2</sub>), 35.94 (alkyl CH), 30.95, 30.56, 28.51, 23.01 (alkyl CH<sub>2</sub>), 14.00, 10.45 (alkyl CH<sub>3</sub>). Anal. calc. for C<sub>28</sub>H<sub>23</sub>F<sub>4</sub>NS: C - 69.55, H -

5.21, N - 2.90 %; found C - 69.51, H - 5.19, N - 2.88 %.  $M_w$  (g mol<sup>-1</sup>): 4,200,  $M_n$ : 2,400, PDI: 1.75. Decomposition temp.: 135 °C.

#### 4.3.4. Co-poly-yne P4

A similar procedure used to synthesize **P1** was followed using **4** and 5,7-dibromo-2,3-diphenylthieno[3,4-b]pyrazine to obtain a yellow solid (65 %). IR (ATR, diamond):  $\nu/\text{cm}^{-1}$  2085 (C≡C). <sup>1</sup>H NMR (700 MHz, CDCl<sub>3</sub>):  $\delta_{\text{H}}/\text{ppm}$  7.56-7.34 (m, 14H, aromatic), 6.89-6.87 (s, 2H, PTZ<sub>H</sub>), 3.79-3.52 (dd, 2H, NCH<sub>2</sub>), 2.19 (s, 1H, CH) 1.60 (s, 1H, CH<sub>2</sub>), 1.57-1.56 (d, 1H, CH<sub>2</sub>), 1.43-1.30 (m, 6H, CH<sub>2</sub>), 0.91-0.89 (b, 6H, CH<sub>3</sub>). <sup>13</sup>C NMR (176 MHz, CDCl<sub>3</sub>):  $\delta_{\text{C}}/\text{ppm}$  153.99, 145.62, 142.42, 138.80, 131.13-128.09, 125.27 (aromatic), 115.94 (C≡C), 51.37 (NCH<sub>2</sub>), 36.02 (alkyl CH), 30.95, 28.51, 23.02, 19.28 (alkyl CH<sub>2</sub>), 14.04, 10.50 (alkyl CH<sub>3</sub>). Anal. calc. for C<sub>40</sub>H<sub>33</sub>N<sub>3</sub>S<sub>2</sub>: C - 77.26, H - 5.67, N - 6.76 %; found: C - 77.18, H - 5.66, N - 6.74 %.  $M_w$  (g mol<sup>-1</sup>): 3,950,  $M_n$ : 2,300, PDI: 1.72. Decomposition temp.: 170 °C.

#### 4.3.5. Co-poly-yne P5

A similar procedure used to synthesize **P1** was followed using **4** and 5,5'-dibromo-2,2'-bithiophene to obtain a yellow solid (57 %). IR (ATR, diamond):  $\nu/\text{cm}^{-1}$  2098 (C≡C). <sup>1</sup>H NMR (700 MHz, CDCl<sub>3</sub>):  $\delta_{\text{H}}/\text{ppm}$  7.53-7.27 (b, 4H, BTh<sub>H</sub>), 7.15-7.10 (m, 4H, PTZ<sub>H</sub>), 7.06-7.05 (d, 1H, PTZ<sub>H</sub>), 6.99-6.98 (d, 1H, PTZ<sub>H</sub>), 3.73 (s, 2H, NCH<sub>2</sub>), 2.16 (s, 1H, CH), 1.55 (s, 2H, CH<sub>2</sub>) 1.44-1.26 (m, 6H, CH<sub>2</sub>), 0.87-0.86 (b, 6H, CH<sub>3</sub>). <sup>13</sup>C NMR (176 MHz, CDCl<sub>3</sub>):  $\delta_{\text{C}}/\text{ppm}$  156.58, 156.52, 142.78, 139.22, 137.23, 129.59, 129.56, 127.70, 127.24, 124.71, 123.38, 121.13, 115.16 (aromatic), 111.96-111.86 (C≡C), 51.37 (NCH<sub>2</sub>), 35.83 (alkyl CH), 30.95, 28.61, 23.14, 22.66 (alkyl CH<sub>2</sub>), 14.97, 10.47 (alkyl CH<sub>3</sub>). Anal. calc. for C<sub>30</sub>H<sub>27</sub>NS<sub>3</sub>: C- 72.10, H - 5.85, N - 2.80 %; found: C - 71.99, H - 5.83, N - 2.77 %.  $M_w$  (g mol<sup>-1</sup>): 16,900,  $M_n$ : 13,800, PDI: 1.22. Decomposition temp.: 133 °C.

#### 4.3.6. Co-poly-yne P6

A similar procedure used to synthesize **P1** was followed using **4** and 4,4'-dibromo-1,1'-biphenyl to obtain a yellow solid (83 %). IR (ATR, diamond):  $\nu/\text{cm}^{-1}$  2088 (C≡C). <sup>1</sup>H NMR (700 MHz, CDCl<sub>3</sub>):  $\delta_{\text{H}}/\text{ppm}$  7.58-7.53 (b, 6H, Ph<sub>H</sub>), 7.47-7.46 (d, 2H, Ph<sub>H</sub>), 7.34-7.30 (m, 4H, PTZ<sub>H</sub>), 6.84-6.78 (m, 2H, PTZ<sub>H</sub>), 3.72 (b, 2H, NCH<sub>2</sub>), 2.17 (s, 1H, CH), 1.57 (s, 2H, CH<sub>2</sub>), 1.43-1.25 (m, 6H, CH<sub>2</sub>), 0.88-0.86 (b, 6H, CH<sub>3</sub>). <sup>13</sup>C NMR (176 MHz, CDCl<sub>3</sub>):  $\delta_{\text{C}}/\text{ppm}$  145.81, 145.03, 139.52, 139.28, 131.98, 131.91, 131.20, 130.46, 128.57, 126.80, 125.30, 125.17, 122.70, 121.90 (aromatic), 116.11-115.82 (C≡C), 51.24 (NCH<sub>2</sub>), 35.94 (alkyl CH), 30.53, 28.46, 23.86, 23.00 (alkyl CH<sub>2</sub>), 13.99, 10.43 (alkyl CH<sub>3</sub>). Anal. calc. for C<sub>34</sub>H<sub>31</sub>NS: C - 83.73, H - 6.82, N - 2.87 %; found: C - 83.7, H - 6.80, N - 2.84 %.  $M_w$  (g mol<sup>-1</sup>): 20,700,  $M_n$ : 13,600, PDI: 1.52. Decomposition temp.: 168 °C.

#### 4.3.7. Co-poly-yne P7

A similar procedure used to synthesize **P1** was followed using **4** and 2,5-dibromothiophene to obtain an orange solid (58 %). IR (ATR, diamond):  $\nu/\text{cm}^{-1}$  2082 (C≡C). <sup>1</sup>H NMR (700 MHz, CDCl<sub>3</sub>):  $\delta_{\text{H}}/\text{ppm}$  7.33-7.29 (m, 4H, PTZ<sub>H</sub>), 7.16-7.15 (d, 1H, Th), 7.12 (s, 1H, PTZ<sub>H</sub>), 6.91-6.90 (d, 1H, Th) 6.85-6.83 (m, 1H, PTZ<sub>H</sub>), 3.76-3.74 (b, 2H, NCH<sub>2</sub>), 2.20 (s, 1H, CH), 1.58 (s, 2H, CH<sub>2</sub>), 1.46-1.25 (m, 6H, CH<sub>2</sub>), 0.90-0.88 (b, 6H,

CH<sub>3</sub>). <sup>13</sup>C NMR (176 MHz, CDCl<sub>3</sub>): δ<sub>C</sub>/ppm 144.43, 136.04, 131.84, 130.53, 129.74, 129.23, 128.59, 124.28, 115.82, 114.86 (aromatic), 93.24, 92.43, 81.46, 80.48 (C≡C), 50.22 (NCH<sub>2</sub>), 34.91 (alkyl CH), 29.53, 27.47, 22.88, 21.98 (alkyl CH<sub>2</sub>), 12.98, 9.44 (alkyl CH<sub>3</sub>). Anal. calc. for C<sub>26</sub>H<sub>25</sub>NS<sub>2</sub>: C - 74.78, H - 6.52, N - 3.35 %; found: C - 74.71, H - 6.50, N - 3.31 %. *M<sub>w</sub>* (g mol<sup>-1</sup>): 6,000, *M<sub>n</sub>*: 4,650, PDI: 1.29. Decomposition temp.: 121 °C.

#### 4.4. Gel-permeation chromatography

Gel permeation chromatography (GPC) was used to characterize the organic poly-ynes. A Viscotek VE2001 GPCmax instrument equipped with a TDA 305 triple detector array was used, which measures refractive index (RI), light scattering both at right angles and low angles (RALS and LALS respectively) and viscosity. A Viscotek 2600 UV detector was also used. Three Polyanalytik SupereRes™ Series 300 mm × 8 mm linear mixed bed columns with linear polystyrene molar mass ranges of 103 to 106 were used for the analysis. The instrument was operated at 35 °C with a THF flow rate of 1 mL min<sup>-1</sup>. The absolute number-average molecular weight (*M<sub>n</sub>*), weight-average molecular weight (*M<sub>w</sub>*) and polydispersity index (*M<sub>w</sub>*/*M<sub>n</sub>*) of the synthesized polymers were obtained by analyzing the chromatograms with the OmniSEC 4.6.1 software. An estimated value of 0.12 for the refractive index increment (*dn/dc*) was used in all cases.

#### 4.5. Computational modelling

Molecular quantum-chemical calculations were carried out on the precursor PTZ core **4** and seven finite-chain model compounds **M1-M7**, approximating **P1-P7**, each consisting of a chain of three PTZ and two spacer moieties with the terminal alkyne groups capped by methyl substituents. The calculations were performed in the gas phase using the density-functional theory (DFT) formalism implemented in the Gaussian09 software.<sup>49</sup> The calculations used the CAM-B3LYP hybrid functional<sup>50</sup> in conjunction with Pople split-valence basis sets<sup>51</sup> of 6-31g and 6-31g\*\* quality for the H and non-H atoms, respectively. Electronic minimization was performed to tolerances of 10<sup>-6</sup> and 10<sup>-8</sup> a.u. on the maximum and root-mean-square (RMS) changes in the density matrix, respectively. Geometry optimizations were performed to tolerances of 4.5 × 10<sup>-4</sup> and 3 × 10<sup>-4</sup> a.u. on the maximum and RMS force and 1.8 × 10<sup>-3</sup> and 1.2 × 10<sup>-3</sup> a.u. on the maximum and RMS displacements, and the optimized structures were confirmed to be stationary points on the potential-energy surface by the absence of negative eigenvalues in the nuclear hessian matrices. Time-dependent DFT (TD-DFT) calculations<sup>52</sup> were performed on the optimized structures to identify the lowest-lying 50 (PTZ) or 150 (**M1-M7**) singlet and triplet states, and selected states were characterized using the method of natural transition orbitals (NTOs).<sup>36</sup> Visualization of the structures, frontier orbitals and NTOs was performed using the VESTA software.<sup>53</sup>

#### 4.6. Electrochemistry measurements

CV measurements were carried out on the polymer modified GCEs in 0.1 M Bu<sub>4</sub>NPF<sub>6</sub>/CH<sub>3</sub>CN solution. For these measurements a standard three-electrode configuration employing a Pt wire counter electrode, the modified GCE working electrode of 3 mm diameter, and an Ag/AgCl non-aqueous reference electrode kit was used (BASi, USA). The Ag/AgCl non-aqueous reference electrode was filled with 0.1 M *n*-Bu<sub>4</sub>NPF<sub>6</sub>

containing ca. 10 mM AgCl to provide a constant reference potential; this was subsequently corrected using 1.0 mM of the ferrocene/ferrocenium potential in the same electrolyte on the day of use as an internal reference. Measurements were performed at a 100 mV s<sup>-1</sup> scan rate at room temperature using a PalmSens3 computer-controlled potentiostat with the PSTrace electrochemistry software (PalmSens BV).

#### 4.7. Polymer light-emitting diode device fabrication and characterization

Device structures consisting of ITO/PEDOT:PSS (40 nm)/TFB (20 nm)/Polymer:PVK (30 nm)/TPBi (20 nm)/LiF (1 nm)/Al (100 nm) were fabricated to assess the performance of the co-poly-ynes as PLED emitters. (ITO - indium tin oxide; PEDOT:PSS - poly(3,4-ethylenedioxythiophene)/ poly(styrenesulfonate); TFB - poly(9,9-dioctylfluorene-co-N-(4-butylphenyl)diphenylamine); PVK - poly(9-vinylcarbazole); TPBi - benzimidazol-2-yl)benzene.) PEDOT:PSS was deposited on the ITO by spin-coating at 3000 rpm under an N<sub>2</sub> atmosphere, and the TFB layer was then deposited by spin-coating under the same conditions. Room-temperature solutions of the co-poly-ynes in chlorobenzene were prepared (**P1/P3/P5-P7** - 10 mg mL<sup>-1</sup>, **P2/P4** - 5 mg mL<sup>-1</sup>) and an emissive layer consisting of the polymers in PVK was deposited by spin-coating at 2000 rpm under N<sub>2</sub>. Concentrations of 5, 10, 15 and 20 wt. % **P7** and 10 wt. % **P1-P6** in PVK were tested. Finally, a 20 nm TPBi layer, a 1 nm LiF cathode and a 100 nm Al capping layer were deposited on top of the emissive layer through a shadow mask under vacuum (2 x 10<sup>-4</sup> Pa). The active area of the devices was 2 mm × 2 mm. The electroluminescence spectra of the devices were measured using an Ocean Optics USB 2000 fiber-optic spectrometer in the normal direction. The *J-V-L* curves were measured using a dual-channel Keithley 2614B source measure unit and a PIN-25D silicon photodiode. All measurements were conducted at room temperature under ambient conditions.

#### 4.8. Polymer solar-cell device fabrication and characterization

Device stacks consisting of ITO/PEDOT:PSS (35 nm)/Polymer:PCBM (70-110 nm)/Ca (20 nm)/Al (80 nm) were fabricated to assess the photovoltaic performance of the co-poly-ynes in bulk heterojunction polymer solar cells. (ITO - indium tin oxide; PEDOT:PSS - poly(3,4-ethylenedioxythiophene)/poly(styrenesulfonate); PCBM - phenyl-C61-butyric acid methyl ester.) [TODO] The active layers were deposited by spin-coating from a 1:1 blend solution (o-dichlorobenzene) of the co-poly-ynes with PCBM with a total concentration of 20 mg mL<sup>-1</sup> at 800-1800 rpm for 60 s, resulting in films with nominal thicknesses of 70-110 nm as determined using a surface profiler (Alfa Step 500, Tencor). After spin-coating, the samples were transferred to an evaporator and the 20 nm Ca and 80 nm Al layers were thermally deposited under vacuum at 10<sup>-6</sup> torr to form the top anode. The current-voltage characteristics of the devices were measured using a Keithley 236 source meter under AM 1.5G illumination at 100 mW cm<sup>-2</sup> produced by a 91160A-1000 solar simulator (Oriel). The external quantum efficiency was measured at a chopping frequency of 275 Hz using a SR830 lock-in amplifier (Stanford Research) under monochromatic illumination from a xenon lamp.

## CRediT

**Idris Juma Al-Busaidi:** Synthesis, Characterization, Investigation, Methodology; **Ashanul Haque:** Funding acquisition, Conceptualization, Investigation, Methodology, Writing - original draft; **Rayya Al-Balushi:** Data curation, Formal analysis; **Jahangir Ahmad Rather:** Data curation, Formal analysis; **Abdul Munam:** Data curation, Formal analysis; **Rashid Ilmi:** Data curation, analysis; **Paul R. Raithby:** Funding acquisition, Writing - review & editing; **Youming Zhang:** Data curation, Formal analysis; **Wai-Yeung Wong:** Funding acquisition, Writing - review & editing; **Jonathan M. Skelton:** Funding acquisition, Investigation, Methodology, Writing - original draft, Writing - review & editing; **Yingying Fu:** Data curation, Formal analysis; **Zhiyuan Xie:** Data curation, Formal analysis; **Shuming Chen:** Data curation, Formal analysis; **Shahidul M Islam:** Data curation, Formal analysis; **Muhammad S. Khan:** Funding acquisition, Conceptualization, Writing - review & editing.

## Conflict of Interest

The authors declare no competing financial interests.

## ACKNOWLEDGEMENTS

MSK thanks the British Petroleum, Oman (Grant EG/SQU-BP/CHI/CHEM/19/01) and the Ministry of Higher Education, Research and Innovation (MoHERI), Oman (Grant RC/RG-SCI/CHEM/20/01) for funding this research work. AH extend his appreciation to the Deputy for Research & Innovation, Ministry of Education in Saudi Arabia for funding part of this research work through the project number RDO-2001. IJAB acknowledges the MoE, Oman for a Ph.D. scholarship. W-YW acknowledges financial support from the Hong Kong Research Grants Council (PolyU 153051/17P), the Hong Kong Polytechnic University (1-ZE1C), Research Institute for Smart Energy (RISE), Ms. Clarea Au for the Endowed Professorship (847S) and the Open Research Fund of State Key Laboratory of Polymer Physics and Chemistry, Changchun Institute of Applied Chemistry, Chinese Academy of Sciences. JMS is currently supported by a UK Research and Innovation Future Leaders Fellowship (MR/T043121/1), and previously held a Presidential Fellowship from the University of Manchester, UK. PRR is grateful to the Engineering and Physical Sciences Research Council (EPSRC) (UK) for continued support (Grant EP/K004956/1). We profoundly thank distinguished Prof. Frank Marken of the Department of Chemistry, University of Bath, UK for helpful discussion on electrochemistry results.

## References

1. C.-L. Ho, Z.-Q. Yu and W.-Y. Wong, *Chem. Soc. Rev.*, 2016, **45**, 5264-5295.
2. A. Haque, R. A. Al-Balushi, I. J. Al-Busaidi, M. S. Khan and P. R. Raithby, *Chem. Rev.*, 2018, **118**, 8474-8597.
3. A. J. Heeger, *Chem. Soc. Rev.*, 2010, **39**, 2354-2371.
4. U. H. Bunz, *Chem. Rev.*, 2000, **100**, 1605-1644.
5. Y. J. Cheng, S. H. Yang and C. S. Hsu, *Chem. Rev.*, 2009, **109**, 5868-5923.
6. A. Haque, L. Xu, R. A. Al-Balushi, M. K. Al-Suti, R. Ilmi, Z. Guo, M. S. Khan, W.-Y. Wong and P. R. Raithby, *Chem. Soc. Rev.*, 2019, **48**, 5547-5563.
7. J. D. L. D. Idris Juma Al-Busaidia, Willyan F. Oliveirab, Ashanul Haque, Nawal K. Al Rasbi, Paul R. Raithby, Muhammed S. Khan, *Dalton Trans.*, 2021, **50**, 1465-1477.
8. A. Haque, R. Al-Balushi, I. J. Al-Busaidi, N. K. Al-Rasbi, S. Al-Bahri, M. K. Al-Suti, O. K. Abou-Zied, M. S. Khan, J. M. Skelton and P. R. Raithby, *Inorg. Chem.*, 2021, **60**, 745-759.



9. L. Wang, L. Yin, L. Wang, B. Xie, C. Ji and Y. Li, *Dyes and Pigments*, 2017, **140**, 203-211.
10. R. Grisorio, G. Allegretta, G. P. Suranna, P. Mastrorilli, A. Lojudice, A. Rizzo, M. Mazzeo and G. Gigli, *J. Mater. Chem. C.*, 2012, **22**, 19752-19760.
11. A. Köhler, M. Younus, M. R. A. Al-Mandhary, P. R. Raithby, M. S. Khan and R. H. Friend, *Syn. Metals*, 1999, **101**, 246-247.
12. M. Jayapal, A. Haque, I. J. Al-Busaidi, R. Al-Balushi, M. K. Al-Suti, S. M. Islam, M. S. Khan and J. Dittmer, *Curr. Org. Chem.*, 2017, **21**, 2017-2027.
13. H.-J. Yun, H. H. Choi, S.-K. Kwon, Y.-H. Kim and K. Cho, *Chem. Mater.*, 2014, **26**, 3928-3937.
14. D.-Y. Chiou, Y.-C. Su, K.-E. Hung, J.-Y. Hsu, T.-G. Hsu, T.-Y. Wu and Y.-J. Cheng, *Chem. Mater.*, 2018, **30**, 7611-7622.
15. Y. Hua, S. Chang, D. Huang, X. Zhou, X. Zhu, J. Zhao, T. Chen, W.-Y. Wong and W.-K. Wong, *Chem. Mater.*, 2013, **25**, 2146-2153.
16. Y. Hua, S. Chang, H. Wang, D. Huang, J. Zhao, T. Chen, W.-Y. Wong, W.-K. Wong and X. Zhu, *J. Power. Sources*, 2013, **243**, 253-259.
17. Y. Hua, L. T. L. Lee, C. Zhang, J. Zhao, T. Chen, W.-Y. Wong, W.-K. Wong and X. Zhu, *J. Mater. Chem. A*, 2015, **3**, 13848-13855.
18. W.-Y. Wong, W.-C. Chow, K.-Y. Cheung, M.-K. Fung, A. B. Djurišić and W.-K. Chan, *J. Organomet. Chem.*, 2009, **694**, 2717-2726.
19. C. H. Siu, L. T. L. Lee, S. C. Yiu, P. Y. Ho, P. Zhou, C. L. Ho, T. Chen, J. Liu, K. Han and W. Y. Wong, *Chem. Euro. J.*, 2016, **22**, 3750-3757.
20. M. Sailer, M. Nonnenmacher, T. Oeser and T. J. Müller, *Euro. J. Org. Chem.*, 2006, **2006**, 423-435.
21. M. Sailer, A. W. Franz and T. J. Müller, *Chem. Euro. J.*, 2008, **14**, 2602-2614.
22. I. J. Al-Busaidi, A. Haque, N. K. Al Rasbi and M. S. Khan, *Synth. Met.*, 2019, **257**, 116189.
23. A. C. B. Rodrigues, J. Pina and J. S. S. de Melo, *J. Mol. Liq.*, 2020, **317**, 113966.
24. V. Quesneau, K. Renault, M. Laly, S. Jenni, F. Ponsot and A. Romieu, *Tetrahedron Lett.*, 2020, **61**, 152582.
25. S. Revoju, A. Matuhina, L. Canil, H. Salonen, A. Hiltunen, A. Abate and P. Vivo, *J. Mater. Chem. C*, 2020, **8**, 15486-15506.
26. R. A. Al-Balushi, A. Haque, M. Jayapal, M. K. Al-Suti, J. Husband, M. S. Khan, O. F. Koentjoro, K. C. Molloy, J. M. Skelton and P. R. Raithby, *Inorg. Chem.*, 2016, **55**, 6465-6480.
27. S. Ergun, C. F. Elliott, A. P. Kaur, S. R. Parkin and S. A. Odom, *Chemical Communications*, 2014, **50**, 5339-5341.
28. D. Shinde, J. K. Salunke, N. R. Candeias, F. Tinti, M. Gazzano, P. Wadgaonkar, A. Priimagi, N. Camaioni and P. Vivo, *Sci. Rep.*, 2017, **7**, 1-10.
29. J. S. Wilson, A. Köhler, R. H. Friend, M. K. Al-Suti, M. R. A. Al-Mandhary, M. S. Khan and P. R. Raithby, *J. Chem. Phys.*, 2000, **113**, 7627-7634.
30. A. Köhler, J. S. Wilson, R. H. Friend, M. K. Al-Suti, M. S. Khan, A. Gerhard and H. Bässler, *J. Chem. Phys.*, 2002, **116**, 9457-9463.
31. M. S. Khan, M. K. Al-Suti, M. R. A. Al-Mandhary, B. Ahrens, J. K. Bjernemose, M. F. Mahon, L. Male, P. R. Raithby, R. H. Friend, A. Köhler and J. S. Wilson, *Dalton Trans.*, 2003, **0**, 65-73.
32. L. Sudha Devi, M. K. Al-Suti, N. Zhang, S. J. Teat, L. Male, H. A. Sparkes, P. R. Raithby, M. S. Khan and A. Köhler, *Macromolecules*, 2009, **42**, 1131-1141.
33. D.-H. Hwang, S.-K. Kim, M.-J. Park, J.-H. Lee, B.-W. Koo, I.-N. Kang, S.-H. Kim and T. Zyung, *Chemistry of Materials*, 2004, **16**, 1298-1303.
34. K. D. Thériault and T. C. Sutherland, *Physic. Chem. Chem. Phys.*, 2014, **16**, 12266-12274.
35. J. M. Skelton, D. S. Gunn, S. Metz and S. C. Parker, *J. Chem. Theory Comput.*, 2020, **16**, 3543-3557.
36. M. Frisch, *J. Chem. Phys.*, 2003, **118**, 4775.

37. C. S. Krämer, K. Zeitler and T. J. J. Müller, *Tetrahedron Letters*, 2001, **42**, 8619-8624.
38. G. Kim, H. R. Yeom, S. Cho, J. H. Seo, J. Y. Kim and C. Yang, *Macromolecules*, 2012, **45**, 1847-1857.
39. X. Kong, A. P. Kulkarni and S. A. Jenekhe, *Macromolecules*, 2003, **36**, 8992-8999.
40. K.-C. Li, Y.-C. Hsu, J.-T. S. Lin, C.-C. Yang, K.-H. Wei and H.-C. Lin, *Journal of Polymer Science Part A: Polymer Chemistry*, 2009, **47**, 2073-2092.
41. Y. Takeda, T. L. Andrew, J. M. Lobez, A. J. Mork and T. M. Swager, *Angewandte Chemie*, 2012, **124**, 9176-9180.
42. A. Bejan, S. Shova, M.-D. Damaceanu, B. C. Simionescu and L. Marin, *Crystal Growth & Design*, 2016, **16**, 3716-3730.
43. A. Tsuboyama, H. Iwawaki, M. Furugori, T. Mukaide, J. Kamatani, S. Igawa, T. Moriyama, S. Miura, T. Takiguchi, S. Okada, M. Hoshino and K. Ueno, *Journal of the American Chemical Society*, 2003, **125**, 12971-12979.
44. C. W. Tang and S. A. VanSlyke, *Applied Physics Letters*, 1987, **51**, 913-915.
45. J. Shi, L. Xu, C. Chen, X. Lv, Q. Ding, W. Li, S. Xue and W. Yang, *Dyes and Pigments*, 2019, **160**, 962-970.
46. C. Schmitz, P. Pösch, M. Thelakkat, H.-W. Schmidt, A. Montali, K. Feldman, P. Smith and C. Weder, *Advanced Functional Materials*, 2001, **11**, 41-46.
47. E. Smarsly, D. Daume, F. Braig, S. Koser, E. Dörsam and U. H. F. Bunz, *Journal of Materials Chemistry C*, 2018, **6**, 11002-11006.
48. J. Shi, L. Xu, X. Lv, Q. Ding, W. Li, Q. Sun, S. Xue and W. Yang, *Dyes and Pigments*, 2019, **161**, 97-103.
49. M. Frisch, G. Trucks, H. Schlegel, G. Scuseria, M. Robb, J. Cheeseman, G. Scalmani, V. Barone, B. Mennucci and G. Petersson, *Journal*, 2009.
50. C. Bannwarth and S. Grimme, *Comp. Theor. Chem.*, 2014, **1040**, 45-53.
51. M. J. Frisch, J. A. Pople and J. S. Binkley, *J. Chem. Phys.*, 1984, **80**, 3265-3269.
52. R. Scuseria, *J. Chem. Phys.*, 1998, **109**, 8218-8224.
53. K. Momma and F. Izumi, *J. Appl. Crystallogr.*, 2011, **44**, 1272-1276.